# 1 Quarkonium in Medium

## 1.1 Quarkonium as probe of hot and dense matter

It is expected that strongly interacting matter shows qualitatively new behavior at temperatures and/or densities which are comparable to or larger than the typical hadronic scale. It has been argued that, under such extreme conditions, deconfinement of quarks and gluons should set in and the thermodynamics of strongly-interacting matter could then be understood in terms of these elementary degrees of freedom. This new form of matter is called *quark-gluon plasma* [1]. The existence of such a transition has indeed been demonstrated from first principles using Monte-Carlo simulations of lattice QCD. The properties of this new state of matter have also been studied [2–5].

In addition to theoretical efforts, the deconfinement transition and the properties of hot, strongly-interacting matter are also studied experimentally in heavy-ion collisions [6, 7]. A significant part of the extensive experimental heavy-ion program is dedicated to measuring quarkonium yields since Matsui and Satz suggested that quarkonium suppression could be a signature of deconfinement [8]. In fact, the observation of anomalous suppression was considered to be a key signature of deconfinement at SPS energies [9].

However, not all of the observed quarkonium suppression in nucleus-nucleus ($AB$) collisions relative to scaled proton-proton ($pp$) collisions is due to quark-gluon plasma formation. In fact, quarkonium suppression was also observed in proton-nucleus ($pA$) collisions, so that part of the nucleus-nucleus suppression is due to cold nuclear matter effects. Therefore, it is necessary to disantangle hot and cold medium effects. We next discuss cold nuclear matter effects at different center-of-mass energies. Then we discuss what is known about the properties of heavy $Q\overline{Q}$ states in hot, deconfined media. Finally, we review recent experimental results on quarkonium production in $pA$ collisions at the SPS and $pp$, d+Au and $AA$ collisions at RHIC.

## 1.2 Cold nuclear matter effects[1]

The baseline for quarkonium production and suppression in heavy-ion collisions should be determined from studies of cold nuclear matter (CNM) effects. The name cold matter arises because these effects are intrinsic to hadron-nucleus interactions where no hot, dense matter effects are expected. There are several cold nuclear matter effects: modifications of the parton distribution functions in the nucleus relative to the nucleon (shadowing) and energy loss of the parton traversing the nucleus before the hard scattering, assumed to be initial-state effects, intrinsic to the nuclear target, and the absorption (destruction) of the quarkonium state as it passes through the nucleus. Since the latter effect occurs after the $Q\overline{Q}$ pair has been produced and while it is traversing the nuclear medium, this absorption is typically referred to as a final-state effect. In addition, the inclusive $J/\psi$ yield includes contributions from $\chi_c$ and $\psi'$ decays to $J/\psi$ at the 30-35% level [10]. While there is some information on the $A$ dependence of $\psi'$ production, the $A$ dependence of $\chi_c$ production is largely unknown [11].

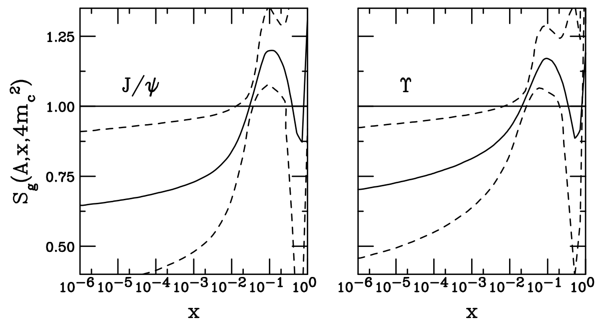


**Fig. 1.** The EPS09 gluon shadowing parameterization [12] at $Q = 2m_c$ and $m_b$. The central value (solid curves) and the associated uncertainty band (dashed curves) are shown.

Even though the contributions to CNM effects may seem rather straightforward, there are a number of associated uncertainties. First, while nuclear modifications to the parton densities are relatively well measured in nuclear deep-inelastic scattering (nDIS), the modifications to the gluon density are not directly measured. The nDIS measurements probe only the quark and antiquark distributions directly. The scaling violations in nDIS can be used to constrain the nuclear gluon density. Overall momentum conservation provides another constraint. However, other, more direct, probes of the gluon density are needed. Current shadowing parameterizations, involving global fits to the nuclear parton densities, give wide variations in the nuclear gluon density from almost no effect to very large low $x$ shadowing compensated by strong antishadowing around $x \sim 0.1$. The range of the possible shadowing effects is illustrated by the new EPS09 parameterization [12] and its associated uncertainties, employing the scale values used to fix the $J/\psi$ and $\Upsilon$ cross sections below the open heavy flavor threshold [13], see Fig. 1.

The color glass condensate (CGC) is expected to play an important role in quarkonium production at RHIC and the LHC since the saturation scale $Q_{S,A}(x)$ is comparable to the charm quark mass [14]. In this picture, collinear factorization of $J/\psi$ production is assumed to break down and forward $J/\psi$ production is suppressed. Indeed, CGC suppression of $J/\psi$ formation may mask some QGP effects [15].

The nuclear absorption survival probability depends on the quarkonium absorption cross section. There are more inherent uncertainties in absorption than in the shadowing parameterization, obtained from data on other processes and is independent of the final state. Typically an absorption cross section is fit to the $A$ dependence of $J/\psi$ and/or $\psi'$ production at a given energy. This is rather simplistic since it is unknown whether the object traversing the nucleus is a precursor state (color octet) which may or may not 'know' what its final identity will be or

[1] C. Lourenco, R. Vogt and H. Wöhri

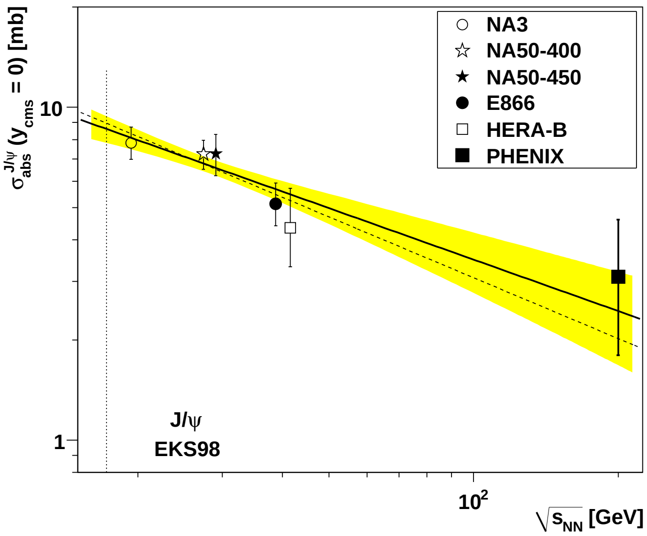


**Fig. 2.** The extracted energy dependence of $\sigma_{\rm abs}^{J/\psi}$ at midrapidity. The solid line is a power law approximations to $\sigma_{\rm abs}^{J/\psi}(y = 0, \sqrt{s_{NN}})$ using the EKS98 [22,23] shadowing parameterization with the CTEQ61L parton densities [24,25]. The band around the exponential curve indicates the uncertainty in the extracted cross sections. The dashed curve shows an exponential fit for comparison. The data at $y_{\rm cms} \sim 0$ from NA3 [26], NA50 at 400 [18] and 450 [19] GeV, E866 [20], HERA-B [27] and PHENIX [28] are also shown. The vertical dotted line indicates the energy of the Pb+Pb and In+In collisions at the CERN SPS. Modified from Ref. [21].

a fully-formed quarkonium state (color singlet). If it is an octet state, it is assumed to immediately interact with a large, finite cross section since it is a colored object [16]. In this case, it has often been assumed that the precursor state is unaware of its final identity so that all quarkonium states will interact with the same cross section. If it is produced as a small color singlet, the absorption cross section immediately after the production of the $Q\overline{Q}$ pair should be small and increasing with proper time until, at the formation time, it reaches its final-state size [17]. High momentum color singlet quarkonium states will experience negligible nuclear absorption effects since they will be formed well outside the target. See Ref. [11] for a discussion of the $A$ dependence of absorption for all the quarkonium states.

Fixed-target data taken in the range $400 \leq E_{\rm lab} \leq 800$ GeV have shown that the $J/\psi$ and $\psi'$ absorption cross sections are not identical, as the basic color octet absorption mechanism would suggest [19,18,20]. The difference between the effective $A$ dependence of $J/\psi$ and $\psi'$ seems to decrease with beam energy. The $J/\psi$ absorption cross section at $x_F \sim 0$ is seen to decrease with energy, regardless of the chosen shadowing parameterization [21], as shown in Fig. 2.

Recent analyses of $J/\psi$ production in fixed-target interactions [21] show that the effective absorption cross section depends on the energy of the initial beam and the rapidity or $x_F$ of the observed $J/\psi$. One possible interpretation is that low momentum color singlet states can hadronize in the target, resulting in larger effective absorption cross sections at lower center of mass energies and backward $x_F$ (or center-of-mass rapidity). At higher energies, the states traverse the target more rapidly so that the $x_F$ values at which they can hadronize in the target move further away from midrapidity and back toward the target (more negative $x_F$). Finally, at sufficiently high energies, the quarkonium states pass through the target before hadronizing, resulting in negligible absorption effects. Thus the *effective* absorption cross section decreases with increasing center-of-mass energy because faster states are less likely to hadronize inside the target.

At higher $x_F$, away from midrapidity, the effective absorption becomes very large, as shown in the top panel of Fig. 3. The increase in $\sigma_{\rm abs}^{J/\psi}$ begins closer to midrapidity for lower incident energies. There appears to be some saturation of the effect since the 800 GeV fixed-target data exhibit the same trend as the most recent (preliminary) PHENIX data [31] as a function of center-of-mass rapidity, $y_{\rm CMS}$, as seen in the bottom panel of Fig. 3. Model calculations including CGC effects can reproduce the general trend of the high $x_F$ behavior of $J/\psi$ production at 800 GeV without invoking energy loss [15]. However, the fact that the NA3 data at $\sqrt{s_{NN}} = 19$ GeV exhibit the same trend in $x_F$ as E866 calls the CGC explanation into question.

As previously discussed, such an increase in the apparent absorption cannot be due to interactions with nucleons. In addition, since the $x_F$ dependence seems to be independent of the quarkonium state (*i.e.* the same for $J/\psi$ and $\psi'$ and also for $\Upsilon(1S)$, $\Upsilon(2S)$ and $\Upsilon(3S)$), it cannot be attributed to the size of the final state and should thus be an initial-state effect. The most likely possibility is initial-state energy loss. (See Ref. [32] for a discussion of several types of energy loss models and their effect on $J/\psi$ production.) Work is in progress to incorporate this effect using a new approach, based on the number of soft collisions the projectile parton undergoes before the hard scattering to produce the $Q\overline{Q}$ pair.

It is also well known that feed down by radiative ($P$ states) and hadronic (higher $S$ states) decays to the $1S$ quarkonium states ($J/\psi$ and $\Upsilon$) account for almost half of all the observed $1S$ final states. These higher-lying quarkonium states have very different sizes and formation times and should thus have different absorption cross sections. For example, the absorption cross section of quarkonium state $C$ may be proportional to its area, $\sigma_C \propto r_C^2$ [33].

It should be noted, however, that the fitted absorption cross sections used for extracting the “normal absorption” baseline for Pb+Pb collisions at the SPS have treated $J/\psi$ and $\psi'$ absorption independently, ignoring feed down and formation times, and have not taken initial-state shadowing into account [19,18]. As discussed above, more detailed analyses show that the quarkonium absorption cross section decreases with increasing energy [34,21]. More recent fixed-target analyses [29,35] have begun to address these issues. When shadowing is included, the extracted absorption cross section is found to be larger at 158 GeV than at

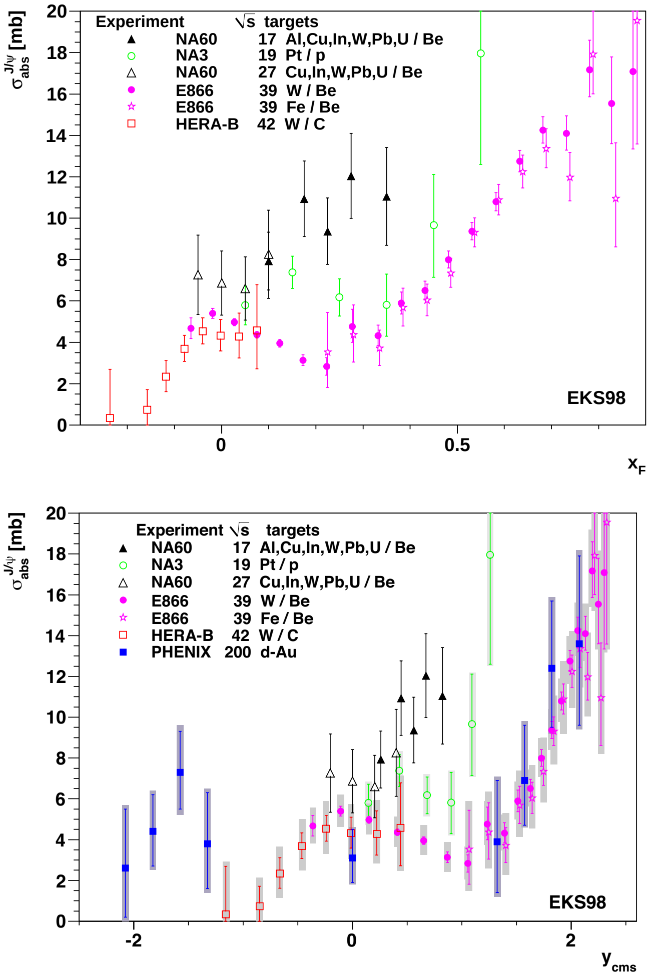


**Fig. 3.** Top: The $x_F$ dependence of $\sigma_{\rm abs}^{J/\psi}$ for incident fixed-target energies from 158 [29] 200 [26], 400 [18], 450 [19], 800 [20] and 920 [27] GeV obtained using the EKS98 shadowing parameterization [22,23]. The E866 [20] and HERA-B [27] results were previously shown in Ref. [21]. Bottom: The same results as above but as a function of center-of-mass rapidity $y_{\rm CMS}$. The absorption cross sections extracted from the preliminary PHENIX results [28] at $|y_{\rm CMS}| > 0$ and the central rapidity result [30] are also included. The boxes around the PHENIX data points show the rapidity-dependent systematic uncertainties.

400 GeV, contrary to previous analyses which assumed a universal, constant absorption cross section [19,18]. When these latest results are extrapolated to nucleus-nucleus collisions at the same energy, the anomalous suppression is significantly decreased relative to the new baseline [29].

The cold nuclear matter effects suggested (initial-state energy loss, shadowing, final-state break-up, *etc.*) depend differently on the quarkonium kinematic variables and the collision energy. It is clearly unsatisfactory to combine all these mechanisms into an *effective* absorption cross section, employed in the Glauber formalism, that only evaluates final-state absorption. Simply taking the $\sigma_{\rm abs}$ obtained from analysis of the $pA$ data and using it to define the Pb+Pb baseline may not be sufficient. Hints that a more complete framework is needed are provided by the observation that the survival probability in S+U collisions is larger than 100% if a stronger $\sigma_{\rm abs}$ value is used, turning the anomalous suppression into an anomalous enhancement, and by the observation of a significant enhancement of $J/\psi$ production in central In+In collisions [29,35,36].

A better understanding of "absorption" requires more detailed knowledge of the production mechanism. Most calculations of the $A$ dependence use the color evaporation model (CEM) where all the quarkonium states are assumed to be produced with the same underlying kinematic distributions [37]. This model works well for fixed-target energies and for RHIC [13], as does the LO color singlet model (CSM) [38] In the latter case, but contrary to the CEM at LO, $J/\psi$ production is necessarily accompanied by the emission of a perturbative final-state gluon which can be seen as an extrinsic source of transverse momentum. This induces modifications in the relations between the initial-state gluon momentum fractions and the momentum of the $J/\psi$. In turn, this modifies [39] the gluon-shadowing corrections relative to those expected from the LO CEM where the transverse momentum of the $J/\psi$ is intrinsic to the initial-state gluons. Further studies are being carried out including the impact of feed down, the extraction of absorption cross sections for each of the charmonium states, and the dependence on the partonic $J/\psi$ production mechanism.

On the other hand, the higher $p_T$ Tevatron data have been calculated within the non-relativistic QCD (NRQCD) approach [40] which includes both singlet and octet matrix elements. These high $p_T$ calculations can be tuned to agree with the high $p_T$ data but cannot reproduce the measured quarkonium polarization at the same energy, see Ref. [41]. If some fraction of the final-state quarkonium yields can be attributed to color singlet production, then absorption need not be solely due to singlet or octet states but some mixture of the two, as dictated by NRQCD [11,42,43]. A measurement of the $A$ dependence of $\chi_c$ production would be particularly helpful to ensure significant progress.

### 1.3 Quarkonium in Hot Medium[2]

#### 1.3.1 Spectral properties of heavy quark anti-quark pair at high temperatures

There has been considerable interest in studying quarkonia in hot medium since publication of the famous Matsui and Satz paper [8]. It has been argued that color screening in a deconfined QCD medium will suppress quarkonium yields, signaling the formation of a quark-gluon plasma (QGP) in heavy-ion collisions. Although this idea was proposed a long time ago, first principle QCD calculations, which go beyond qualitative arguments, have been performed only recently. Such calculations include lattice QCD determinations of quarkonium correlators [44–48]; potential model calculations of the quarkonium spectral functions with potentials based on lattice QCD [49–56];

[2] A. Mocsy and P. Petreczky

as well as effective field theory approaches that justify potential models and reveal new medium effects [57–60]. Furthermore, better modeling of quarkonium production in the medium created in heavy-ion collisions has been achieved. These advancements make it possible to disentangle the cold and hot-medium effects on the quarkonium states, crucial for the interpretation of heavy-ion data.

### 1.3.2 Color screening and deconfinement

At high temperatures, strongly-interacting matter undergoes a deconfining transition to a quark-gluon plasma (QGP). This transition is triggered by a rapid increase of the energy and entropy densities, as well as the disappearance of hadronic states. (For a recent review, see Ref. [4].) According to current lattice calculations, at zero net baryon density deconfinement occurs at $T \sim 170 - 195)$ MeV [4]. The QGP is characterized by color screening: the range of interaction between heavy quarks becomes inversely proportional to the temperature. Thus at sufficiently high temperatures, it is impossible to produce a bound state between a heavy quark ($c$ or $b$) and its antiquark.

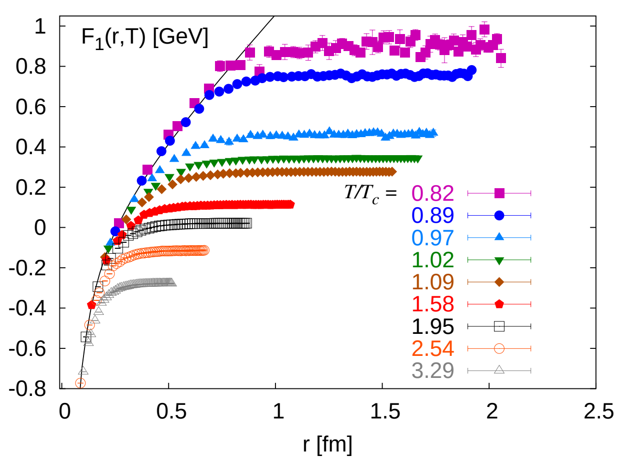


**Fig. 4.** Heavy quark singlet free energy versus quark separation calculated in 2+1 flavor QCD on $16^3 \times 4$ lattices at different temperatures [61,62].

Color screening is studied on the lattice by calculating the spatial correlation function of a static quark and antiquark in a color singlet state which propagates in Euclidean time from $\tau = 0$ to $\tau = 1/T$ where $T$ is the temperature (see Ref. [63] for a recent review). The logarithm of this correlation function, the singlet free energy, is shown in Fig. 4. As expected, in the zero temperature limit the singlet free energy coincides with the zero temperature potential. Figure 4 also illustrates that, at sufficiently short distances, the singlet free energy is temperature independent and equal to the zero temperature potential. The range of interaction decreases with increasing temperature. For temperatures above the transition temperature, $T_c$, the heavy quark interaction range becomes comparable to the charmonium radius. Based on this general observation, one would expect that the charmonium states, as well as the excited bottomonium states, do not remain bound at temperatures just above the deconfinement transition. (In the literature, this is often referred to as dissociation or melting.)

### 1.3.3 Quarkonium spectral functions

In-medium quarkonium properties are encoded in the corresponding spectral functions, as are their dissolution at high temperatures. Spectral functions are defined as the imaginary part of the retarded correlation function of quarkonium operators. Bound states appear as peaks in the spectral functions. The peaks broaden and eventually disappear with increasing temperature. The disappearance of a peak signals the melting of the given quarkonium state.

In lattice QCD, the meson correlation functions, $G(\tau, T)$, are calculated in Euclidean time. These correlation functions are related to the spectral functions $\sigma(\omega, T)$ as

$$G(\tau, T) = \int_0^\infty d\omega \sigma(\omega, T) \frac{\cosh(\omega(\tau - 1/(2T)))}{\sinh(\omega/(2T))} . \qquad (1)$$

Detailed information on $G(\tau, T)$ could make it possible to reconstruct the spectral function from the lattice data. In practice, however, this turns out to be very difficult task because the time extent is limited to $1/T$, see the discussion in Ref. [47] and references therein.

The quarkonium spectral functions can be calculated in potential models using the singlet free energy from Fig. 4 or with different lattice-based potentials obtained using the singlet free energy as an input [55,56,64]. The results of calculations in quenched QCD are shown in Fig. 5 for $S$-wave charmonium (top) and bottomonium (bottom) spectral functions [55]. All charmonium states are dissolved in the deconfined phase while the bottomonium $1S$ state may persist up to $T \sim 2T_c$. The temperature dependence of the Euclidean correlators can be predicted using Eq. (1) and the calculated spectral functions. Somewhat surprisingly, the Euclidean correlation functions show very little temperature dependence irrespective of whether a state remains bound (the $\Upsilon$ $1S$) or not (the $J/\psi$). Note also that correlators from potential models are in accord with the lattice calculations (see insets in Fig. 5). Initially, the weak temperature dependence of the correlators was considered to be evidence for the survival of different quarkonium states [46]. It is now clear that this conclusion was premature.

There is a large enhancement in the threshold region of the spectral functions relative to the free spectral function, as shown in Fig. 5. This threshold enhancement compensates for the absence of bound states and leads to Euclidean correlation functions with very weak temperature dependencies [55]. It further indicates strong residual correlations between the quark and antiquark, even in the absence of bound states. Similar analyses were done for the $P$-wave charmonium and bottomonium spectral functions [55,56]. An upper bound on the dissociation temperature (the temperatures above which no bound states

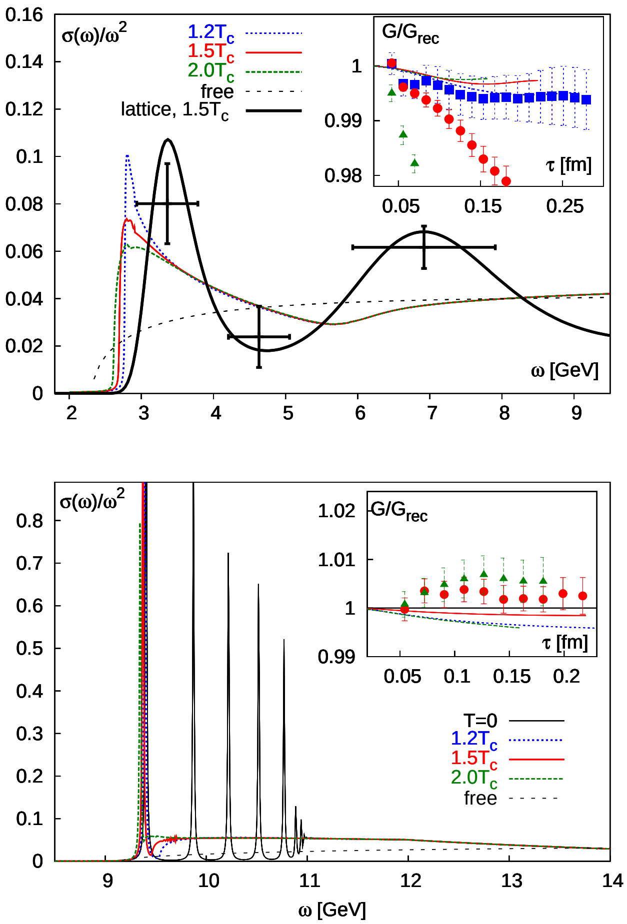


**Fig. 5.** The $S$-wave charmonium (upper) and bottomonium (lower) spectral functions calculated in potential models [55]. Insets: correlators compared to lattice data. The dotted curves are the free spectral functions.

peaks can be seen in the spectral function and bound state formation is suppressed) can be obtained from the analysis of the spectral functions. Conservative upper limits on the dissociation temperatures for the different quarkonium states obtained from a full QCD calculation [56] are given in Table 1.

| State | $\chi_c$ | $\psi'$ | $J\psi$ | $\Upsilon'$ | $\chi_b$ | $\Upsilon$ |
|---|---|---|---|---|---|---|
| $T_{diss}$ | $\leq T_c$ | $\leq T_c$ | $1.2T_c$ | $1.2T_c$ | $1.3T_c$ | $2T_c$ |

**Table 1.** *Upper bounds* on the dissociation temperatures [56].

The application of potential models can be justified using an effective field theory approach. The energy scales related to the heavy quark mass $m$, the inverse size $mv$ (where $v$ is the heavy quark velocity), and the binding energy $mv^2$ makes it possible to construct a sequence of effective theories at zero temperature. The effective theory which emerges after integrating out the scales $m$ and $mv^2$ is pNRQCD, equivalent to the potential model at $T = 0$. It is possible to extend this approach to finite temperature where additional scales, the temperature $T$, the Debye mass $m_D \sim gT$, and the magnetic scale $g^2T$ are present.

In the weak coupling regime, $g \ll 1$, these scales are well separated. Depending on how the thermal scales are related to the zero temperature scales, the various hierarchies make it possible to derive different effective theories for quarkonium bound states at finite temperature [60]. In the weak-coupling QCD approach, thermal corrections to the potential are obtained when the temperature is larger than the binding energy. An important general result of these effective theories is that the potential acquires an imaginary part. The imaginary part of the potential smears out the bound state peaks of the quarkonium spectral function, leading to their dissolution prior to the onset of Debye-screening in the real part of the potential (see *e.g.* the discussion in Ref. [59]).

Most recently, the effects of possible medium anisotropies on the quarkonium states have been considered, both on the real [65] and imaginary [66,67] parts of the potential as well as on bound state production in the real part of the potential [68]. $P$-state polarization has been predicted to arise from the medium anisotropy, including a significant ($\sim 30\%$) effect on the $\chi_b$ states [68]. A weak medium anisotropy may be related to the shear viscosity [69] so that the predicted polarization directly probes the properties of the medium produced in heavy-ion collisions.

### 1.3.4 Dynamical models for quarkonium production

While knowing the quarkonium spectral functions in equilibrium QCD is necessary, it is insufficient to predict effects on their production in heavy-ion collisions because, unlike the light degrees of freedom, heavy quarks are fully thermalized in heavy-ion collisions. Therefore, it is nontrivial to relate the finite temperature quarkonium spectral functions to quarkonium production rates in heavy-ion collisions without further model assumptions. The bridge between the two is provided by dynamical models of the matter produced in heavy-ion collisions. Some of the simple models currently available are based on statistical recombination [70]; statistical recombination and dissociation rates [71]; or sequential melting [72]. Here we highlight a more recent model, which makes closer contact with both QCD and experimental observations [73].

The bulk evolution of the matter produced in heavy-ion collisions is well modeled by hydrodynamics, see Ref. [74] for a recent review. The large heavy quark mass makes it possible to model its interaction with the medium by Langevin dynamics [75]. Such an approach successfully describes the anisotropic flow of charm quarks observed at RHIC [75]. Potential models have shown that, in the absence of bound states, the $Q\overline{Q}$ pairs are correlated in space [55,56]. This correlation can be modeled classically using Langevin dynamics, including a drag force and a random force between the $Q$ (or $\overline{Q}$) and the medium as well as the forces between the $Q$ and $\overline{Q}$ described by the potential. It was recently shown that a model combining an ideal hydrodynamic expansion of the medium with a description of the correlated $Q\overline{Q}$ pair dynamics by the Langevin equation can describe charmonium suppression at RHIC quite well [73]. In particular, this model can explain why, despite the fact that a deconfined medium is created at RHIC, there is only a $40 - 50\%$ suppression in the charmonium yield. The attractive potential and the finite lifetime of the system prevents the complete decorrelation of some of the $Q\overline{Q}$ pairs [73]. Once the matter has cooled sufficiently, these residual correlations make it possible for the $Q$ and $\overline{Q}$ to form a bound state.

The above approach, which neglects quantum effects, is applicable only if there are no bound states, as is likely to be the case for the $J/\psi$. If heavy quark bound states are present, as is probable for the $\Upsilon(1S)$, the thermal dissociation rate will be most relevant for understanding the quarkonium yield. It is expected that the interaction of a color singlet quarkonium state with the medium is much smaller than that of heavy quarks. Thus, to first approximation, medium effects will only lead to quarkonium dissociation.

### 1.3.5 Finite temperature summary

Potential model calculations based on lattice QCD, as well as resummed perturbative QCD calculations, indicate that all charmonium states and the excited bottomonium states dissolve in the deconfined medium. This leads to the reduction of the quarkonium yields in heavy-ion collisions compared to the binary-scaling of $pp$ collisions. Recombination and edge effects, however, guarantees a non-zero yield.

One of the great opportunities of the LHC and RHIC-II heavy-ion programs is the ability to study bottomonium yields. From a theoretical perspective, bottomonium is an important and clean probe for at least two reasons. First, the effective field theory approach, which provides a link to first principles QCD, is more applicable for bottomonium due to better separation of scales and higher dissociation temperatures. Second, the heavier bottom quark mass reduces the importance of recombination effects, making bottomonium a good probe of dynamical models.

## 1.4 Recent results at SPS energies[3]

### 1.4.1 Introduction

In recent years, studies of charmonium production and suppression in cold and hot nuclear matter have been carried out by the NA60 collaboration [29,76,77]. In particular, data have been taken for In+In collisions at 158 GeV/nucleon and for $pA$ collisions at 158 and 400 GeV. In the following, the primary NA60 results and their impact on the understanding of the anomalous $J/\psi$ suppression, first observed by the NA50 collaboration in Pb+Pb collisions [78], are summarized. Finally, a preliminary comparison between the suppression patterns observed at the SPS and RHIC are discussed.

[3] E. Scomparin, R. Arnaldi and P. Cortese

## 1.5 $J/\psi$ production in $pA$ collisions at 158 and 400 GeV

One of the main results of the SPS heavy-ion program was the observation of anomalous $J/\psi$ suppression. Results obtained in Pb+Pb collisions at 158 GeV/nucleon by the NA50 collaboration showed that, in such collisions, the $J/\psi$ yield was suppressed with respect to estimates that include only cold nuclear matter effects [78]. The magnitude of the cold nuclear matter effects has typically been extracted by extrapolating the $J/\psi$ production data obtained in $pA$ collisions. Until recently the reference SPS $pA$ data were based on samples collected at 400/450 GeV by the NA50 collaboration, at higher energy than the nuclear collisions and in a slightly different rapidity domain [19, 18,79].

The need for reference $pA$ data taken under the same conditions as the $AA$ data was a primary motivation for the NA60 experiment. A run with an SPS primary proton beam at 158 GeV was carried out in 2004. Seven nuclear targets (Be, Al Cu, In, W, Pb, and U) were simultaneously exposed to the beam. The sophisticated NA60 experimental set-up [80], based on a high-resolution vertex spectrometer coupled to the muon spectrometer inherited from NA50, made it possible to unambiguously identify the target in which the primary interaction occurred as well as measure muon pairs from the $J/\psi$ decay with a $\sim 70$ MeV invariant mass resolution. During the same period, a 400 GeV $pA$ data sample was taken with the same experimental set-up.

Cold nuclear matter effects have been evaluated comparing the cross section ratio $\sigma_{pA}^{J/\psi}/\sigma_{p\mathrm{Be}}^{J/\psi}$, for each nucleus with mass number $A$, relative to the lightest target (Be). The beam luminosity factors cancel out in the ratio, apart from a small beam attenuation factor. However, since the sub-targets see the vertex telescope from slightly different angles, the track reconstruction efficiencies do not completely cancel out. Therefore an accurate evaluation of the time evolution of such quantities was performed target by target, with high granularity, down to the single pixel level, and on a run-per-run basis. The results [29,77], shown in Fig. 6, are integrated over $p_T$ and are given in the rapidity region covered by all the sub-targets, $0.28 < y_{\mathrm{CMS}} < 0.78$ for the 158 GeV sample and $-0.17 < y_{\mathrm{CMS}} < 0.33$ for the 400 GeV sample. Systematic errors include uncertainties in the target thickness, the rapidity distribution used in the acceptance calculation, and the reconstruction efficiency. Only the fraction of systematic errors not common to all the points is shown since it affects the evaluation of nuclear effects.

Nuclear effects have usually been parameterized by fitting the $A$ dependence of the $J/\psi$ production cross section using the expression $\sigma_{pA}^{J/\psi} = \sigma_{pp}^{J/\psi} A^{\alpha}$. Alternatively, the effective absorption cross section, $\sigma_{\mathrm{abs}}^{J/\psi}$ can be extracted from the data using the Glauber model. Both $\alpha$ and $\sigma_{\mathrm{abs}}^{J/\psi}$ are effective quantities since they represent the strength of the cold nuclear matter effects that reduce the $J/\psi$ yield. However, they cannot distinguish between the different effects, *e.g.* shadowing and nuclear absorption, contributing

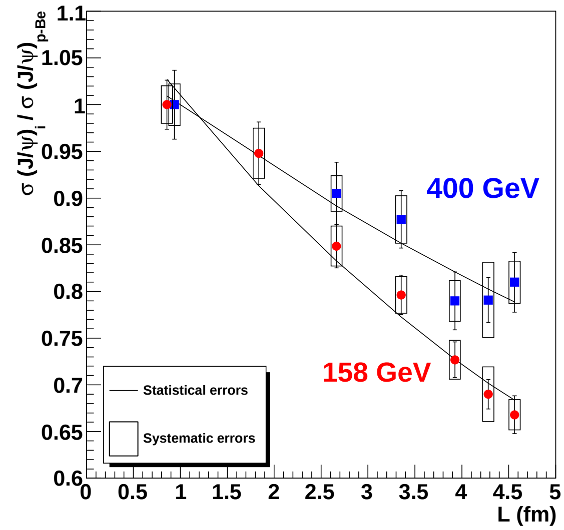


**Fig. 6.** The $J/\psi$ cross section ratios for $pA$ collisions at 158 GeV (circles) and 400 GeV (squares), as a function of $L$, the mean thickness of nuclear matter traversed by the $J/\psi$.

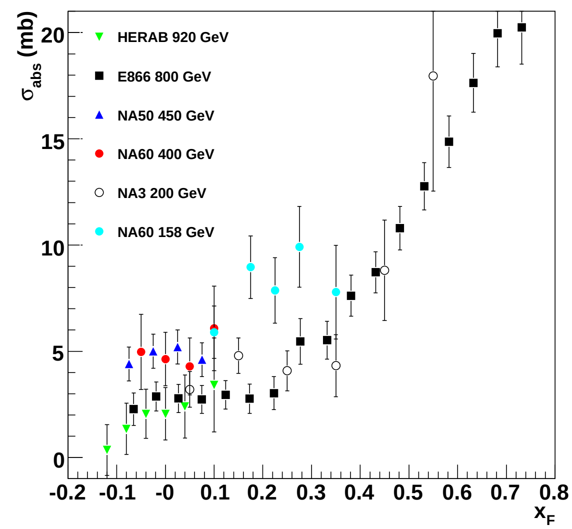


**Fig. 7.** Compilation of $\sigma_{\rm abs}^{J/\psi}$ as a function of $x_F$ with no additional cold matter effects included.

to this reduction. The results in Fig. 6 were used to extract $\sigma_{\rm abs}^{J/\psi} = 7.6 \pm 0.7\,({\rm stat.}) \pm 0.6\,({\rm syst.})$ mb (corresponding to $\alpha = 0.882 \pm 0.009 \pm 0.008$) at 158 GeV and $\sigma_{\rm abs}^{J/\psi} = 4.3 \pm 0.8\,({\rm stat.}) \pm 0.6({\rm syst.})$ mb ($\alpha = 0.927 \pm 0.013 \pm 0.009$)) at 400 GeV. Thus $\sigma_{\rm abs}^{J/\psi}$ is larger at 158 GeV than at 400 GeV. The 400 GeV result is, on the other hand, in excellent agreement with the previous NA50 result obtained at the same energy [18].

The study of cold nuclear matter effects at fixed-target energies is a subject which has attracted considerable interest. In Fig. 7, a compilation of previous results for $\sigma_{\rm abs}^{J/\psi}$ as a function of $x_F$ [19,20,26,27] is presented, together with the new NA60 results [77]. The only cold nuclear matter effect included in the extraction of $\sigma_{\rm abs}^{J/\psi}$ is absorption. There is a systematic increase in the nuclear effects going from low to high $x_F$ as well as when from high to low incident proton energies. As shown in Fig. 7, the new NA60 results at 400 GeV confirm the NA50 values obtained at a similar energy. On the other hand, the NA60 158 GeV data suggest higher values of $\sigma_{\rm abs}^{J/\psi}$ as well a hint of increased absorption over the $x_F$ range. Note also that the older NA3 $J/\psi$ results are in partial contradiction with these observations, giving lower values of $\sigma_{\rm abs}^{J/\psi}$, similar to those obtained from the higher energy data samples. Such a complex pattern of nuclear effects results from a delicate interplay of various nuclear effects (final state absorption, shadowing, initial state energy loss *etc.*) and has so far not been satisfactorily explained by theoretical models [32]. A first attempt at disentangling the contribution of shadowing from the effective absorption cross section $\sigma_{\rm abs}^{J/\psi}$ extracted from the NA60 results has been carried out, correcting the measured cross section ratios for the shadowing factors calculated using the EKS98 [23] parameterization of the nuclear PDFs. It was found that a larger $\sigma_{\rm abs}^{J/\psi}$ is needed to describe the measured data, $\sigma_{\rm abs}^{J/\psi}(158\,{\rm GeV}) = 9.3 \pm 0.7 \pm 0.7$ mb and $\sigma_{\rm abs}^{J/\psi}(400\,{\rm GeV}) = 6.0 \pm 0.9 \pm 0.7$ mb, compare with the values of $\sigma_{\rm abs}^{J/\psi}$ in the upper plot of Fig. 3 extracted including the EKS98 parameterization. Note that the values of $\sigma_{\rm abs}^{J/\psi}$ extracted for the E866 data around $x_F \approx 0$ are flatter when no shadowing is included. The results depend on the parameterization of the nuclear modifications of the PDFs. For example, slightly higher values of $\sigma_{\rm abs}^{J/\psi}$ (on the $\sim 5-10\%$ level) are obtained if the EPS08 [81] parameterization is used.

### 1.5.1 Anomalous $J/\psi$ suppression in In+In and Pb+Pb collisions

The $pA$ results at 158 GeV shown in the previous section have been collected at the same energy and in the same $x_F$ range of the SPS $AA$ data. It is therefore natural to use these results to calculate the expected magnitude of cold nuclear matter effects on $J/\psi$ production in nuclear collisions. In order to do so, the expected shape of the $J/\psi$ distribution as a function of the forward energy $E_{\rm ZDC}$, $dN_{{\rm J}/\psi}^{\rm expect}/dE_{\rm ZDC}$, has been determined using the Glauber model. The $J/\psi$ yield is assumed to scale with the number of $NN$ collisions. The $J/\psi$ absorption cross section in nuclear matter is assumed to be the same as the value at 158 GeV deduced in the previous section.

The measured forward $J/\psi$ yield, $dN_{{\rm J}/\psi}/dE_{\rm ZDC}$, is normalized to $dN_{{\rm J}/\psi}^{\rm expect}/dE_{\rm ZDC}$ using the procedure detailed in Ref. [76]. This procedure previously did not take shadowing effects into account when extrapolating from $pA$ to $AA$ interactions. In $pA$ collisions, only the target

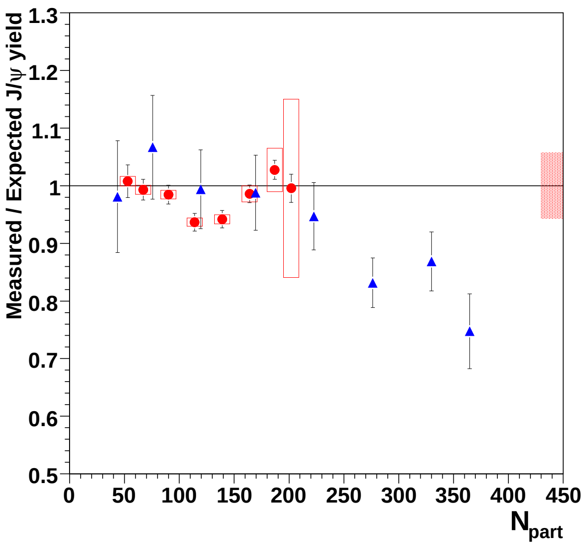


**Fig. 8.** Anomalous $J/\psi$ suppression in In+In (circles) and Pb+Pb collisions (triangles), as a function of $N_{\rm part}$. The boxes around the In+In points represent correlated systematic errors. The filled box on the right-hand side corresponds to the uncertainty in the absolute normalization of the In+In points. A 12% global error, due to the uncertainty on $\sigma_{\rm abs}^{J/\psi}$ at 158 GeV is not shown.

partons are affected by shadowing while in $AA$ collisions, effects on both the projectile and target must be taken into acount. If shadowing is neglected in the $pA$ to $AA$ extrapolation, a small bias is introduced, resulting in an artificial $\sim$ 5% suppression of the $J/\psi$ yield with the EKS98 parameterization [35]. Therefore, if shadowing is properly accounted for in the $pA$ to $AA$ extrapolation, the amount of the anomalous $J/\psi$ suppression is reduced. Figure 8 presents the new results for the anomalous $J/\psi$ suppression in In+In and Pb+Pb collisions [29,77] as a function of $N_{\rm part}$, the number of participant nucleons. Up to $N_{\rm part} \sim 200$ the $J/\psi$ yield is, within errors, compatible with the extrapolation of cold nuclear matter effects. When $N_{\rm part} > 200$, there is an anomalous suppression of up to $\sim 20-30\%$ in the most central Pb+Pb collisions. The new, smaller, anomalous suppression is primarily due to the larger $\sigma_{\rm abs}^{J/\psi}$ extracted from the evaluation of cold nuclear matter effects.

## 1.6 Recent Quarkonia results from RHIC[4]

### 1.6.1 Introduction

The strategy of the RHIC $J/\psi$ program has been to measure production cross sections in $\sqrt{s_{_{NN}}} = 200$ GeV collisions for $pp$, d+Au, Au+Au and Cu+Cu collisions. The $pp$ collisions are studied both to learn about the $J/\psi$ production mechanism and to provide baseline production cross sections needed for understanding the d+Au and $AA$ data. Similarly, the d+Au measurements are inherently interesting because they study the physical processes that modify $J/\psi$ production cross sections in nuclear targets and also provide the crucial cold nuclear matter baseline for understanding $J/\psi$ production in $AA$ collisions. Note that d+Au collisions are studied at RHIC instead of $p$+Au collisions for convenience - $p$+Au collisions are possible at RHIC, but would require a dedicated $p$+Au run.

The last few years of the RHIC program have produced $J/\psi$ data from PHENIX for $pp$, d+Au and Au+Au collisions with sufficient statistical precision to establish the centrality dependence of both hot and cold nuclear matter effects at $\sqrt{s_{_{NN}}} = 200$ GeV. The data cover the rapidity range $|y| < 2.4$.

In the next few years the increased RHIC luminosity and the commissioning of upgraded detectors and triggers for PHENIX and STAR will enable a next generation of RHIC measurements, extending the program to the $\Upsilon$ family, excited charmonium states, and $J/\psi$ $v_2$ and high $p_T$ suppression measurements. There have already been low precision, essentially proof of principle, measurements of most of those signals. Very importantly, upgraded silicon vertex detectors for both PHENIX and STAR are expected to produce qualitatively better open charm measurements that will provide important inputs to models of $J/\psi$ production in heavy-ion collisions.

In addition to the results discussed here, there have been PHENIX results on $J/\psi$ photoproduction in peripheral Au+Au collisions [82] and a proof-of-principle measurement of the $J/\psi$ $v_2$ in Au+Au collisions by PHENIX [83] with insufficient precision for physics conclusions.

### 1.6.2 Results on charmonium production from $pp$ collisions

PHENIX has recently reported preliminary measurements of the inclusive $J/\psi$ polarization in 200 GeV $pp$ collisions at midrapidity [84]. Results for the polarization parameter $\lambda$, defined in the Helicity frame, shown in Fig. 9, are compared with a color-octet (COM) prediction [85] and the $s$-channel cut Color Singlet Model [86] which has been shown to describe the rapidity and $p_T$ dependence of the PHENIX 200 GeV $pp$ $J/\psi$ data [87], using two parameters fit to CDF data at $\sqrt{s} = 1.8$ TeV.

At Quark Matter 2009, PHENIX showed preliminary measurements of the $p_T$ dependence of the $\psi'$ cross section at 200 GeV [28]. This is the first measurement of the $p_T$ dependence of an excited charmonium state at RHIC. PHENIX measured the feed-down contribution of the $\psi'$ to the $J/\psi$ to be $8.6 \pm 2.3\%$, in good agreement with the world average.

STAR has recently published measurements [88] of the $J/\psi$ cross section in 200 GeV $pp$ collisions for $p_T$ from 5 to 13 GeV/$c$. This greatly extends the $p_T$ range over which $J/\psi$ data are available at RHIC. Although PHENIX can trigger at all $p_T$, it has so far been limited to $p_T$ below about 9 GeV/$c$ [28] because of its much smaller acceptance.

[4] A.D. Frawley

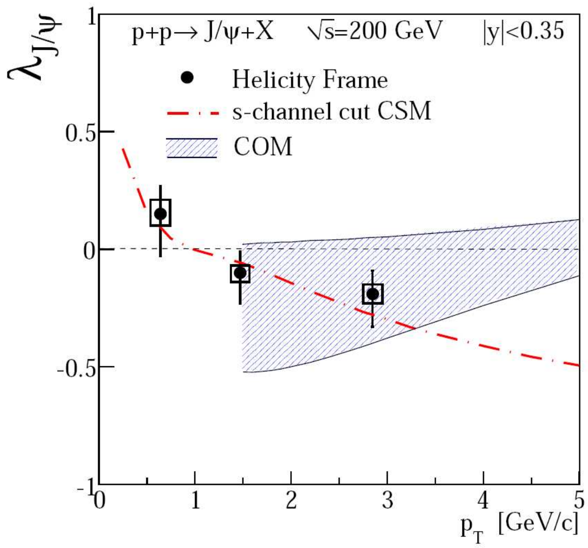


**Fig. 9.** The polarization extracted from 200 GeV PHENIX $pp$ data at midrapidity as a function of $p_T$. The data are compared with the $s$-channel cut CSM [86] and a Color Octet Model prediction [85].

### 1.6.3 Results on charmonium production from Cu+Cu collisions at high $p_T$

PHENIX results on the rapidity and $p_T$ dependence of the $J/\psi$ $R_{AA}$ from 200 GeV Cu+Cu collisions were published some time ago [89]. However those results were limited to $p_T < 5$ GeV/$c$, and do not address the high $p_T$behavior of the $J/\psi$ $R_{AA}$ very well. STAR has now published [88] Cu+Cu $J/\psi$ $R_{AA}$ data at 5.5 and 7 GeV/$c$ that yield an average $R_{AA}$ of $1.4 \pm 0.4(stat) \pm 0.2(sys)$ above 5 GeV/$c$ for the 0-20% most central collisions. The $R_{AA}$ data for the 0-60% most central collisions have very similar values, in contrast to the PHENIX $R_{AA}$ data below 5 GeV/$c$ that yield an average $R_{AA}$ of 0.52 for central Cu+Cu collisions.

PHENIX has also released preliminary data for the $J/\psi$ $R_{AA}$ from minimum bias (0-94% centrality) Cu+Cu data at 7 and 9 GeV/$c$ [83]. The minimum bias PHENIX data should be comparable to the STAR 0-60% data, but the PHENIX results are more consistent with a nearly $p_T$-independent $R_{AA}$. However, both measurements have large statistical uncertainties and a direct comparison of the STAR and PHENIX Cu+Cu $R_{AA}$ data at high $p_T$ [90] suggests that, while they disagree, more data will be required to definitively determine the high $p_T$ behavior of the $R_{AA}$ in central collisions.

### 1.6.4 Results on $\Upsilon(1S) + \Upsilon(2S) + \Upsilon(3S)$ production

PHENIX showed a preliminary result [91] for the $\Upsilon(1S) + \Upsilon(2S) + \Upsilon(3S)$ cross section at forward and backward rapidity ($1.2 < |y| < 2.4$) at Quark Matter 2006. More recently, PHENIX showed a preliminary result at Quark Matter 2009 for $\Upsilon(1S) + \Upsilon(2S) + \Upsilon(3S)$ production in 200 GeV $pp$ collisions at midrapidity ($|y| < 0.35$) [28]. The measured cross section is $Bd\sigma/dy = 114^{+46}_{-45}$ pb at $y = 0$.

The STAR experiment has recently published a measurement of the $\Upsilon(1S) + \Upsilon(2S) + \Upsilon(3S) \to e^+e^-$ cross section at $|y| < 0.5$ for 200 GeV $pp$ collisions [92]. The measured value is $Bd\sigma/dy = 114 \pm 38\,(\text{stat.})^{+23}_{-24}\,(\text{syst})$pb at $y = 0$. STAR also has a preliminary result for the $\Upsilon(1S)+\Upsilon(2S)+\Upsilon(3S) \to e^+e^-$ cross section at midrapidity [93] in d+Au collisions at 200 GeV/$c$. The cross section was found to be $Bd\sigma/dy = 35 \pm 4\,(\text{stat}) \pm 5\,(\text{syst})$ nb. The midrapidity value of $R_{\text{dAu}}$ was found to be $0.98 \pm 0.32\,(\text{stat}) \pm 0.28\,(\text{syst})$, consistent with binary scaling.

PHENIX has made a preliminary measurement of the dielectron yield in the $\Upsilon(1S)+\Upsilon(2S)+\Upsilon(3S)$ mass range at midrapidity in Au+Au collisions [83]. In combination with the PHENIX $\Upsilon(1S) + \Upsilon(2S) + \Upsilon(3S)$ $pp$ result at midrapity, a 90% CL upper limit on $R_{\text{dAu}}$ of 0.64 was found for the $\Upsilon(1S) + \Upsilon(2S) + \Upsilon(3S)$ mass region. The significance of this result is not yet very clear since the measurement is for all three $\Upsilon$ states combined.

### 1.6.5 Results on $J/\psi$ production from d+Au collisions

As discussed previously, modification of the $J/\psi$ production cross section due to the presence of a nuclear target is expected to be caused by shadowing, breakup of the precursor $J/\psi$ state by collisions with nucleons, initial-state energy loss and, possibly, other effects. Parameterizing these effects by employing a Glauber model with a fitted effective $J/\psi$ absorption cross section, $\sigma_{\text{abs}}^{J/\psi}$, results in an effective cross section with strong rapidity and $\sqrt{s_{NN}}$ dependencies [21] that are not well understood. A large increase in the effective absorption cross section is observed at forward rapidity [20] that cannot be explained by shadowing models alone, suggesting that there are important physics effects left out of the Glauber absorption + shadowing model.

The extraction of hot matter effects in the Au+Au $J/\psi$ data at RHIC has been seriously hampered by the poor understanding of $J/\psi$ production in nuclear targets, including the underlying $J/\psi$ production mechanism. Thus the cold nuclear matter baseline has to be obtained experimentally.

The PHENIX $J/\psi$ data obtained in the 2003 RHIC d+Au run did not have sufficient statistical precision either for studies of cold nuclear matter effects, or for a cold nuclear matter baseline reference for the Au+Au data [30]. This low statistics measurement has been augmented by the large $J/\psi$ data set obtained in the 2008 d+Au run. PHENIX has released d+Au $R_{CP}$ data for $J/\psi$ production [28] in nine rapidity bins over $|y| < 2.4$. Systematic uncertainties associated with the beam luminosity, detector acceptance, trigger efficiency, and tracking efficiency cancels when $R_{CP}$, the ratio of central to peripheral events, if formed. There is a remaining systematic uncertainty due to the centrality dependence of the tracking and particle identification efficiencies.

However, there are significant systematic uncertainties in the centrality dependence of $R_{CP}$ due to the use

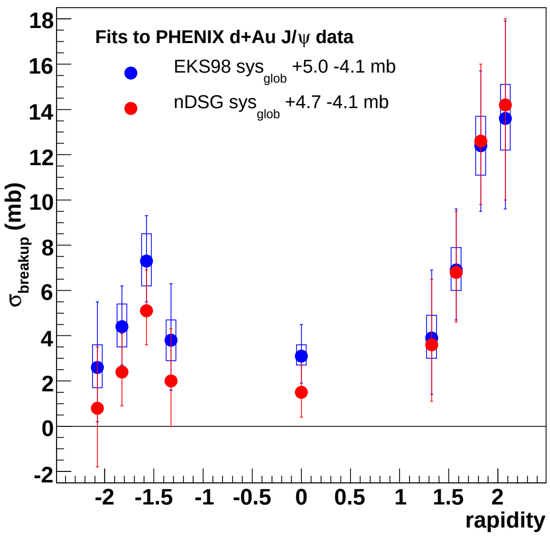


**Fig. 10.** The effective absorption cross section as a function of rapidity extracted from PHENIX d+Au $R_{CP}$ data using the EKS98 and nDSg shadowing parameterizations. The vertical bars show uncorrelated point-to-point uncertainties, the boxes show correlated uncertainties, and the global uncertainties are given in the legend.

of a Glauber model to calculate the average number of nucleon-nucleon collisions as a means of estimating the relative normalization between different centrality bins. The systematic uncertainty due to the Glauber calculation is independent of rapidity.

The PHENIX d+Au $R_{CP}$ data have been independently fitted at each of the nine rapidities [31] employing a model including shadowing and $J/\psi$ absorption. The model calculations [94] use the EKS98 and nDSg shadowing parameterizations with $0 \leq \sigma_{\rm abs} \leq 15$ mb. The best fit absorption cross section was determined at each rapidity, along with the $\pm 1\sigma$ uncertainties associated with a) rapidity-dependent systematic uncertainties and b) rapidity-independent systematic uncertainties.

The results are shown in Fig. 10. The most notable feature is the stronger effective absorption cross section at forward rapidity, similar to the behavior observed at lower energies [20]. In fact, it is striking that the extracted cross sections at forward rapidity are very similar for PHENIX ($\sqrt{s_{NN}} = 200$ GeV) and for the E866 collaboration ($\sqrt{s_{NN}} = 38.8$ GeV) [21], see the lower panel of Fig. 3, despite the large difference in center-of-mass energy.

Note the large global systematic uncertainty in $\sigma_{\rm abs}$ extracted from the PHENIX $R_{CP}$ data, dominated by the uncertainty in the Glauber estimate of the average number of collisions at each centrality. Although it does not affect the shape of the rapidity dependence of $\sigma_{\rm abs}^{J/\psi}$, it results in considerable uncertainty in the magnitude of the effective absorption cross section.

It was recently suggested [95] that the large increase in effective absorption cross section at forward rapidity obtained in [31], obtained from a CEM, calculation, may be moderated significantly if the $2 \to 2$ kinematics of the leading-order CSM is used. This difference emphasizes the importance of understanding the underlying production mechanism.

### 1.6.6 Results on $J/\psi$ production in Au+Au collisions

PHENIX has published the centrality dependence of $R_{AA}$ for Au+Au collisions using Au+Au data from the 2004 RHIC run and *pp* data from the 2005 run [96]. The data are shown in Fig.11. The suppression is considerably stronger at forward rapidity than at midrapidity. The significance of this difference with respect to hot matter effects is not clear, however, unless the suppression due to cold nuclear matter effects is better known.

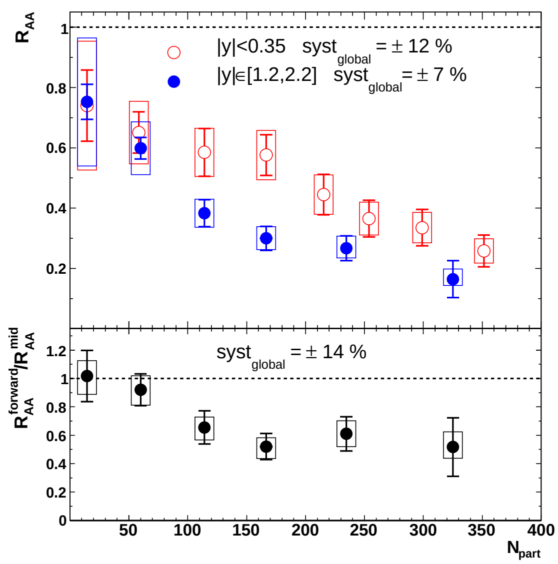


**Fig. 11.** The PHENIX Au+Au $R_{AA}$ as a function of centrality for $|y| < 0.35$ and $1.2 < |y| < 2.2$.

To estimate the cold nuclear matter contribution to the Au+Au $J/\psi$ $R_{AA}$ the d+Au $J/\psi$ $R_{CP}$ data were extracted using the EKS98 and nDSg shadowing parameterizations, as described earlier, exception that, in this case, the $\sigma_{\rm abs}^{J/\psi}$ values in d+Au collisions were fitted independently in three rapidity intervals: $-2.2 < y < -1.2$; $|y| < 0.35$ and $1.2 < y < 2.2$. In effect, this tunes the calculations to reproduce the d+Au $R_{CP}$ independently in each of the three rapidity windows in which the Au+Au $R_{AA}$ data were measured. The cold nuclear matter $R_{AA}$ for Au+Au collisions was then estimated in a Glauber calculation using the fitted absorption cross sections and the centrality-dependent $R_{p{\rm Au}}$ calculated using EKS98 and nDSg shadowing parameterizations [97].

Each nucleon-nucleon collision contributes differently to the $R_{AA}$ in each rapidity window. The analysis assumes that $R_{AA}$ can be treated as a convolution of $p$+Au and Au+$p$ collisions in the three rapidity windows to more directly simulate nucleon-nucleus interactions. The impact parameter dependence of $R_{p\mathrm{Au}}$ is determined separately to infer the $R_{AA}$ centrality dependence for a rapidity-dependent absorption cross section. Thus the value of $R_{p\mathrm{Au}}$ at the impact parameter of nucleon 1 in the projectile is convoluted with the value of $R_{\mathrm{Au}p}$ at the impact parameter of nucleon 2 in the target. Effectively, this means that, to obtain $R_{AA}$ for $1.2 < |y| < 2.2$, $R_{p\mathrm{Au}}$ for the forward-moving nucleon ($1.2 < y < 2.2$) is multiplied by $R_{p\mathrm{Au}}$ for the backward-moving nucleon ($-2.2 < y < -1.2$). When $|y| < 0.35$, the $R_{p\mathrm{Au}}$ calculations at midrapidity are used. The number of participants, obtained from a Glauber calculation, is used to bin the collisions in centrality with a cut on peripheral events to mimic the effect of the PHENIX trigger efficiency at large impact parameter. The uncertainty in the calculated CNM $R_{AA}$ was estimated by repeating the calculation with the best fit $\sigma_{\mathrm{abs}}^{J/\psi}$ values varied within the rapidity-dependent systematic uncertainty determined when fitting the d+Au $R_{CP}$.

The global systematic uncertainty in $\sigma_{\mathrm{abs}}^{J/\psi}$ was neglected in the calculation of the CNM $R_{AA}$ because the number of nucleon-nucleon collisions, $N_{coll}$, in d+Au and Au+Au interactions and the fitted $\sigma_{\mathrm{abs}}^{J/\psi}$ values used to estimate the CNM $R_{AA}$are all obtained using the same Glauber model. Therefore if (for example) $N_{coll}$ is underestimated for the d+Au $R_{CP}$, the fitted absorption cross section will be overestimated. However, this would be compensated in the calculated CNM $R_{AA}$ by the underestimated $N_{coll}$ value. Any possible differences in the details of the d+Au and Au+Au Glauber calculations would result in an imprecise cancelation of the uncertainties. This effect has not yet been studied.

Note that there is a significant difference between the impact parameter dependence of the $R_{p\mathrm{Au}}$ and $R_{\mathrm{dAu}}$ calculations [31], primarily for peripheral collisions, due to the smearing caused by the finite size of the deuteron. Since $R_{\mathrm{dAu}}$ and $R_{p\mathrm{Au}}$ are calculated using the same basic model, this smearing does not present a problem in the present analysis. However, if the measured $R_{\mathrm{dAu}}$ was used directly in a Glauber model, as was done with the RHIC 2003 data in Ref. [30], a correction would be necessary.

The resulting Glauber calculations of the cold nuclear matter $R_{AA}$ using the EKS98 shadowing parameterization are shown in Fig. 12. The values obtained with nDSg are almost identical, as they should be since both parameterize the same d+Au $R_{CP}$ data.

We emphasize that the kinematic-dependent differences in the effective absorption cross sections noted in the previous section do not affect the cold nuclear matter $R_{AA}$ derived from the data. As long as the method of fitting the d+Au data is consistent with the estimate of the cold nuclear matter $R_{AA}$, the result should be model independent.

The $J/\psi$ suppression beyond CNM effects in Au+Au collisions can be estimated by dividing the measured $R_{AA}$ by the estimates of the CNM $R_{AA}$. The result for EKS98 is shown in Fig. 13. The result for nDSg is nearly identical.

It is possible to use the effective absorption cross sections obtained from the d+Au $J/\psi$ $R_{CP}$ data in a similar Glauber calculation of $R_{p\mathrm{Cu}}$ to estimate the cold nuclear

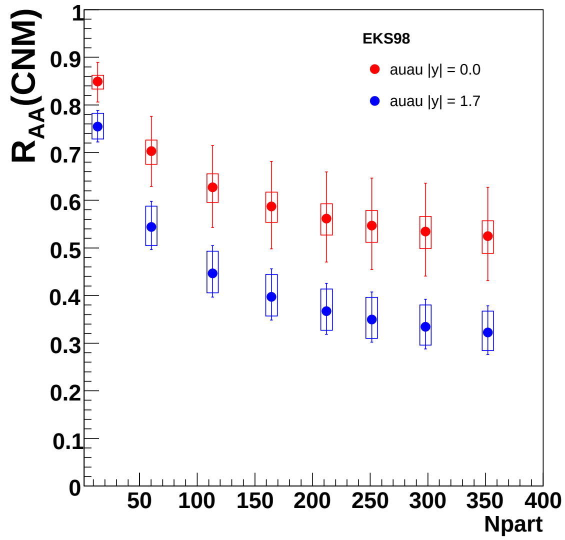


**Fig. 12.** The estimated Au+Au cold nuclear matter $R_{AA}$ as a function of centrality for $|y| < 0.35$ and $1.2 < |y| < 2.2$. The vertical bar represents the rapidity-dependent systematic uncertainty in the fitted $\sigma_{\mathrm{abs}}^{J/\psi}$.

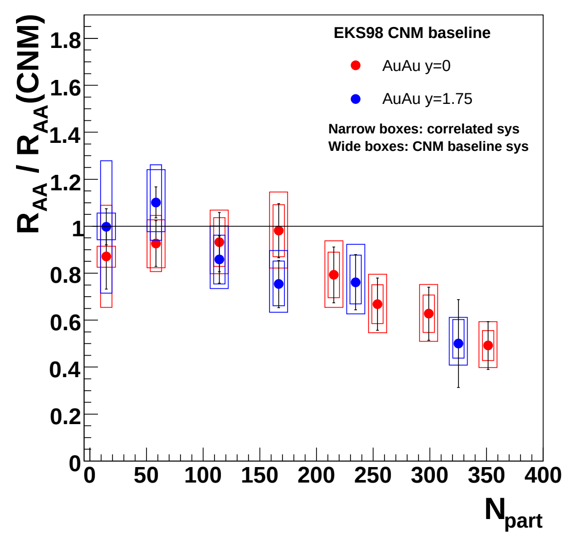


**Fig. 13.** The estimated Au+Au suppression relative to the cold nuclear matter $R_{AA}$ as a function of centrality for $|y| < 0.35$ and $1.2 < |y| < 2.2$. The systematic uncertainty of the baseline cold nuclear matter $R_{AA}$ is depicted by the wide box around each point. The narrow box is the systematic uncertainty in the Au+Au $R_{AA}$.

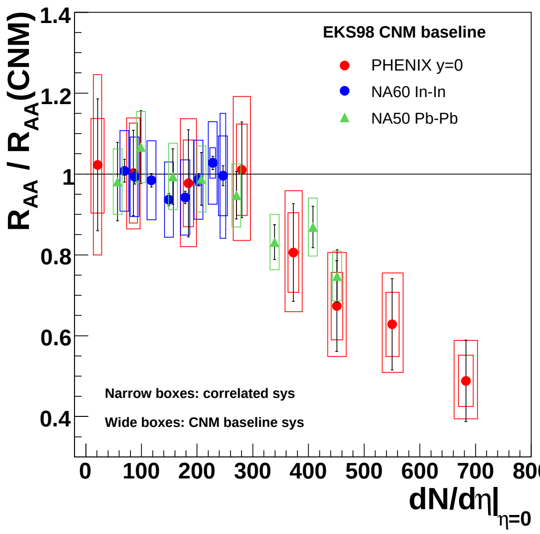


**Fig. 14.** Comparison of the anomalous suppression at the SPS and RHIC as a function of $dN_{\rm ch}/d\eta$ at $\eta = 0$.

matter $R_{AA}$ for Cu+Cu collisions. However, the resulting CNM $R_{AA}$ for Cu+Cu is significantly different for EKS98 and nDSg [31], most likely due to the different $A$ dependence of EKS98 and nDSg. Measurements of $J/\psi$ production in $p$+Cu or d+Cu collisions would be needed to reduce the model dependence of the estimated CNM $R_{AA}$ for Cu+Cu collisions.

#### 1.6.7 Anomalous suppression: SPS vs RHIC[5]

The preliminary PHENIX d+Au results at $\sqrt{s} = 200$ GeV are, for the first time, based on a high-statistics sample [31]. Comparing these results with the previous Au+Au data gives an estimate of the magnitude of the anomalous $J/\psi$ suppression at RHIC. The newly availabile NA60 $pA$ results at 158 GeV, described in Section 1.4, allows a significant comparison between the centrality dependence of the anomalous suppression at the SPS and at RHIC. Work is in progress to make such a comparison as a function of several variables of interest such as the charged particle multiplicity, $dN_{\rm ch}/d\eta$, and the Bjorken energy density reached in the collision. The anomalous suppression patterns in In+In and Pb+Pb collisions at the SPS and the midrapidity Au+Au results at RHIC are presented as a function of $dN_{\rm ch}/d\eta$ in Fig. 14 [98]. Note that the magnitude of the anomalous $J/\psi$ suppression is practically system and $\sqrt{s}$-independent when expressed as a function of $dN_{\rm ch}/d\eta|_{\eta=0}$.

### 1.7 Summary of RHIC results[6]

The last two years of the RHIC program have produced results from $pp$ collisions on $J/\psi$ polarization as well as $\psi'$ and $\Upsilon(1S)+\Upsilon(2S)+\Upsilon(3S)$ production, all measurements new to RHIC. There have also been the first measurements of $\Upsilon(1S)+\Upsilon(2S)+\Upsilon(3S)$ production in d+Au and Au+Au collisions; measurements of the $J/\psi$ $p_T$ distributions up to 13 GeV/$c$ in $pp$ collisions; and measurements of the $J/\psi$ $R_{AA}$ in Cu+Cu collisions for $p_T \geq 5$ GeV/$c$. While all these measurements are statistically challenged, these first results reflect the fact that RHIC is moving into a new regime of increased luminosity and detector performance.

The statistical precision of the 2008 RHIC d+Au $J/\psi$ data set is sufficient for a meaningful estimate of the cold nuclear matter contribution to the $J/\psi$ $R_{AA}$, using a parameterization of the d+Au $R_{CP}$ data by a shadowing model and an effective $J/\psi$ absorption cross section independently fit at mid, forward and backward rapidity. The sharp rise of the effective absorption cross section at forward rapidity fit to the RHIC d+Au data is very similar to that seen at lower center-of-mass energies, see Fig. 3. The increased absorption cross section at forward rapidity leads to greater $J/\psi$ cold nuclear matter suppression in $R_{AA}$ for Au+Au at forward/backward rapidity, as seen in Fig. 12.

When the measured Au+Au $R_{AA}$ is divided by the estimated cold nuclear matter $R_{AA}$, the resulting suppression pattern is found to be very similar at midrapidity and at forward/backward rapidity, as shown in Fig. 13. This conclusion is independent of the shadowing parameterization used, as long as the effective absorption cross section is independently fit to the d+Au $R_{CP}$ data at mid, forward and backward rapidity.

Assuming that the final PHENIX $R_{\rm dAu}$ confirms the strong suppression at forward rapidity seen in $R_{CP}$, it would suggest that the stronger suppression seen at forward/backward rapidity in the PHENIX Au+Au $R_{AA}$ data is primarily due to cold nuclear matter effects. The suppression due to hot matter effects seems to be comparable at midrapidity and at forward/backward rapidity.

## Acknowledgements

We thank the Institute for Nuclear Theory at the University of Washington for hospitality and the Department of Energy for partial support (GRANT NOS) during the completion of this work. The work of R. Vogt was performed under the auspices of the U.S. Department of Energy by Lawrence Livermore National Laboratory under Contract DE-AC52-07NA27344 and was also supported in part by the National Science Foundation Grant NSF PHY-0555660.

## References

1. E. V. Shuryak, Phys. Rept. **61** (1980) 71.

[5] E. Scomparin, R. Arnaldi and P. Cortese

[6] A. D. Frawley

2. P. Petreczky, Nucl. Phys. A **830** (2009) 11C [arXiv:0908.1917 [hep-ph]];
3. Z. Fodor and S. D. Katz, arXiv:0908.3341 [hep-ph];
4. C. DeTar and U. M. Heller, Eur. Phys. J. A **41**, 405 (2009) [arXiv:0905.2949 [hep-lat]];
5. P. Petreczky, Nucl. Phys. Proc. Suppl. **140** (2005) 78 [arXiv:hep-lat/0409139].
6. H. Satz, Rept. Prog. Phys. **63** (2000) 1511 [arXiv:hep-ph/0007069];
7. B. Muller and J. L. Nagle, Ann. Rev. Nucl. Part. Sci. **56**, 93 (2006) [arXiv:nucl-th/0602029].
8. T. Matsui and H. Satz, Phys. Lett. B **178** (1986) 416.
9. CERN press release "New State of Matter created at CERN" Feb. 10, 2000 http://press.web.cern.ch/press/PressReleases/Releases2000/PR01.00EQuarkGluonMatter.html
10. P. Faccioli, C. Lourenco, J. Seixas and H. K. Woehri, JHEP **0810** (2008) 004 [arXiv:0809.2153 [hep-ph]].
11. R. Vogt, Nucl. Phys. A **700** (2002) 539 [arXiv:hep-ph/0107045].
12. K. J. Eskola, H. Paukkunen and C. A. Salgado, JHEP **0904** (2009) 065 [arXiv:0902.4154 [hep-ph]].
13. A. D. Frawley, T. Ullrich and R. Vogt, Phys. Rept. **462** (2008) 125 [arXiv:0806.1013 [nucl-ex]].
14. D. Kharzeev and K. Tuchin, Nucl. Phys. A **735** (2004) 248 [arXiv:hep-ph/0310358].
15. D. Kharzeev, E. Levin, M. Nardi and K. Tuchin, Phys. Rev. Lett. **102** (2009) 152301 [arXiv:0808.2954 [hep-ph]].
16. D. Kharzeev and H. Satz, Phys. Lett. B **366** (1996) 316 [arXiv:hep-ph/9508276].
17. J. P. Blaizot and J. Y. Ollitrault, Phys. Lett. B **217** (1989) 386.
18. B. Alessandro *et al.* [NA50 Collaboration], Eur. Phys. J. C **48** (2006) 329 [arXiv:nucl-ex/0612012].
19. B. Alessandro *et al.* [NA50 Collaboration], Eur. Phys. J. C **33** (2004) 31.
20. M. J. Leitch *et al.* [FNAL E866/NuSea collaboration], Phys. Rev. Lett. **84** (2000) 3256 [arXiv:nucl-ex/9909007].
21. C. Lourenco, R. Vogt and H. K. Woehri, JHEP **0902** (2009) 014 [arXiv:0901.3054 [hep-ph]].
22. K. J. Eskola, V. J. Kolhinen and P. V. Ruuskanen, Nucl. Phys. B **535** (1998) 351 [arXiv:hep-ph/9802350].
23. K. J. Eskola, V. J. Kolhinen and C. A. Salgado, Eur. Phys. J. C **9** (1999) 61 [arXiv:hep-ph/9807297].
24. J. Pumplin, D. R. Stump, J. Huston, H. L. Lai, P. M. Nadolsky and W. K. Tung, JHEP **0207** (2002) 012 [arXiv:hep-ph/0201195].
25. D. Stump, J. Huston, J. Pumplin, W. K. Tung, H. L. Lai, S. Kuhlmann and J. F. Owens, JHEP **0310** (2003) 046 [arXiv:hep-ph/0303013].
26. J. Badier *et al.* [NA3 Collaboration], Z. Phys. C **20** (1983) 101.
27. I. Abt *et al.* [HERA-B Collaboration], Eur. Phys. J. C **60** (2009) 525 [arXiv:0812.0734 [hep-ex]].
28. C. L. da Silva [PHENIX Collaboration], Nucl. Phys. A **830** (2009) 227c [arXiv:0907.4696 [nucl-ex]].
29. E. Scomparin [NA60 Collaboration], Nucl. Phys. A **830** (2009) 239c [arXiv:0907.3682 [nucl-ex]].
30. A. Adare *et al.* [PHENIX Collaboration], Phys. Rev. C **77** (2008) 024912 [Erratum-ibid. C **79** (2009) 059901] [arXiv:0711.3917 [nucl-ex]].
31. A. D. Frawley, talk at ECT* workshop on Quarkonium Production in Heavy-Ion Collisions, Trento (Italy), May 25-29, 2009 and at Joint CATHIE-INT mini-program "Quarkonia in Hot QCD", June 16-26, 2009 http://www.int.washington.edu/talks/WorkShops/int_09_42W.
32. R. Vogt, Phys. Rev. C **61** (2000) 035203 [arXiv:hep-ph/9907317].
33. B. Povh and J. Hufner, Phys. Rev. Lett. **58** (1987) 1612.
34. R. Vogt, Phys. Rev. C **71** (2005) 054902 [arXiv:hep-ph/0411378].
35. R. Arnaldi, P. Cortese and E. Scomparin, Phys. Rev. C **81** (2010) 014903 [arXiv:0909.2199 [hep-ph]].
36. C. Lourenco, talk at ECT* workshop on Quarkonium Production in Heavy-Ion Collisions, Trento (Italy), May 25-29, 2009 and at Joint CATHIE-INT mini-program "Quarkonia in Hot QCD", June 16-26, 2009 http://www.int.washington.edu/talks/WorkShops/int_09_42W.
37. R. Gavai, D. Kharzeev, H. Satz, G. A. Schuler, K. Sridhar and R. Vogt, Int. J. Mod. Phys. A **10** (1995) 3043 [arXiv:hep-ph/9502270].
38. S. J. Brodsky and J. P. Lansberg, arXiv:0908.0754 [hep-ph].
39. E. G. Ferreiro, F. Fleuret, J. P. Lansberg and A. Rakotozafindrabe, Phys. Lett. B **680** (2009) 50 [arXiv:0809.4684 [hep-ph]].
40. G. T. Bodwin, E. Braaten and G. P. Lepage, Phys. Rev. D **51** (1995) 1125 [Erratum-ibid. D **55** (1997) 5853] [arXiv:hep-ph/9407339].
41. N. Brambilla *et al.* [Quarkonium Working Group], arXiv:hep-ph/0412158.
42. M. Beneke and I. Z. Rothstein, Phys. Rev. D **54** (1996) 2005 [Erratum-ibid. D **54** (1996) 7082] [arXiv:hep-ph/9603400].
43. X. F. Zhang, C. F. Qiao, X. X. Yao and W. Q. Chao, arXiv:hep-ph/9711237.
44. T. Umeda, K. Nomura and H. Matsufuru, Eur. Phys. J. C **39S1** (2005) 9 [arXiv:hep-lat/0211003].
45. M. Asakawa and T. Hatsuda, Phys. Rev. Lett. **92**, 012001 (2004);
46. S. Datta, F. Karsch, P. Petreczky and I. Wetzorke, Phys. Rev. D **69**, 094507 (2004) [arXiv:hep-lat/0312037].
47. A. Jakovác, P. Petreczky, K. Petrov and A. Velytsky, Phys. Rev. D **75** (2007) 014506 [arXiv:hep-lat/0611017].
48. G. Aarts *et al.*, Phys. Rev. D **76** (2007) 094513 [arXiv:0705.2198 [hep-lat]].
49. S. Digal, P. Petreczky and H. Satz, Phys. Rev. D **64** (2001) 094015 [arXiv:hep-ph/0106017].
50. C. Y. Wong, Phys. Rev. C **72** (2005) 034906.
51. Á. Mócsy and P. Petreczky, Phys. Rev. D **73** (2006) 074007 [arXiv:hep-ph/0512156].
52. Eur. Phys. J. C **43** (2005) 77 [arXiv:hep-ph/0411262].
53. W. M. Alberico, A. Beraudo, A. De Pace and A. Molinari, Phys. Rev. D **75** (2007) 074009.
54. D. Cabrera and R. Rapp, Phys. Rev. D **76** (2007) 114506 [arXiv:hep-ph/0611134].
55. Á. Mócsy and P. Petreczky, Phys. Rev. D **77** (2008) 014501 [arXiv:0705.2559 [hep-ph]].
56. Á. Mócsy and P. Petreczky, Phys. Rev. Lett. **99** (2007) 211602 [arXiv:0706.2183 [hep-ph]].
57. M. Laine, O. Philipsen and M. Tassler, JHEP **0709** (2007) 066 [arXiv:0707.2458 [hep-lat]].
58. M. Laine, JHEP **0705** (2007) 028 [arXiv:0704.1720 [hep-ph]].
59. M. Laine, Nucl. Phys. A **820** (2009) 25C [arXiv:0810.1112 [hep-ph]].
60. N. Brambilla, J. Ghiglieri, A. Vairo and P. Petreczky, Phys. Rev. D **78** (2008) 014017 [arXiv:0804.0993 [hep-ph]].

61. O. Kaczmarek, F. Karsch, F. Zantow and P. Petreczky, Phys. Rev. D **70** (2004) 074505 [Erratum-ibid. D **72** (2005) 059903] [arXiv:hep-lat/0406036].
62. K. Petrov [RBC-Bielefeld Collaboration], PoS **LAT2006** (2006) 144 [arXiv:hep-lat/0610041].
63. A. Bazavov, P. Petreczky and A. Velytsky, arXiv:0904.1748 [hep-ph].
64. A. Mocsy, arXiv:0811.0337 [hep-ph].
65. A. Dumitru, Y. Guo and M. Strickland, Phys. Lett. B **662**, 37 (2008) [arXiv:0711.4722 [hep-ph]].
66. A. Dumitru, Y. Guo and M. Strickland, Phys. Rev. D **79** (2009) 114003 [arXiv:0903.4703 [hep-ph]].
67. Y. Burnier, M. Laine and M. Vepsalainen, Phys. Lett. B **678** (2009) 86 [arXiv:0903.3467 [hep-ph]].
68. A. Dumitru, Y. Guo, A. Mocsy and M. Strickland, Phys. Rev. D **79** (2009) 054019 [arXiv:0901.1998 [hep-ph]].
69. M. Asakawa, S. A. Bass and B. Muller, Phys. Rev. Lett. **96** (2006) 252301 [arXiv:hep-ph/0603092].
70. A. Andronic, P. Braun-Munzinger, K. Redlich and J. Stachel, Nucl. Phys. A **789** (2007) 334 [arXiv:nucl-th/0611023].
71. X. Zhao and R. Rapp, Phys. Lett. B **664** (2008) 253 [arXiv:0712.2407 [hep-ph]].
72. F. Karsch, D. Kharzeev and H. Satz, Phys. Lett. B **637** (2006) 75 [arXiv:hep-ph/0512239].
73. C. Young and E. Shuryak, Phys. Rev. C **79** (2009) 034907 [arXiv:0803.2866 [nucl-th]].
74. D. Teaney, arXiv:0905.2433 [nucl-th].
75. G. D. Moore and D. Teaney, Phys. Rev. C **71** (2005) 064904 [arXiv:hep-ph/0412346].
76. R. Arnaldi *et al.* [NA60 Collaboration], Phys. Rev. Lett. **99** (2007) 132302.
77. R. Arnaldi [NA60 Collaboration], Nucl. Phys. A **830** (2009) 345c [arXiv:0907.5004 [nucl-ex]].
78. B. Alessandro *et al.* [NA50 Collaboration], Eur. Phys. J. C **39**, 335 (2005) [arXiv:hep-ex/0412036].
79. B. Alessandro *et al.* [NA50 Collaboration], Phys. Lett. B **553**, 167 (2003).
80. R. Arnaldi *et al.* [NA60 Collaboration], Eur. Phys. J. C **59** (2009) 607 [arXiv:0810.3204 [nucl-ex]].
81. K. J. Eskola, H. Paukkunen and C. A. Salgado, JHEP **0807** (2008) 102 [arXiv:0802.0139 [hep-ph]].
82. S. Afanasiev *et al.* [PHENIX Collaboration], Phys. Lett. B **679** (2009) 321 [arXiv:0903.2041 [nucl-ex]].
83. E. T. Atomssa [PHENIX Collaboration], Nucl. Phys. A **830** (2009) 331c, [arXiv:0907.4787v2 [nucl-ex]].
84. A. Adare *et al.* [PHENIX Collaboration], arXiv:0912.2082 [hep-ex].
85. H. S. Chung, S. Kim, J. Lee and C. Yu, arXiv:0911.2113 [hep-ph].
86. Phys. Rev. Lett. **100** (2008) 032006 [arXiv:0709.3471 [hep-ph]].
87. J. P. Lansberg and H. Haberzettl, AIP Conf. Proc. **1038** (2008) 83 [arXiv:0806.4001 [hep-ph]].
88. B. I. Abelev *et al.* [STAR Collaboration], Phys. Rev. C **80** (2009) 041902 [arXiv:0904.0439 [nucl-ex]].
89. A. Adare *et al.* [PHENIX Collaboration], Phys. Rev. Lett. **101** (2008) 122301 [arXiv:0801.0220 [nucl-ex]].
90. L. A. Linden Levy, Nucl. Phys. A **830** (2009) 353c [arXiv:0908.2361 [nucl-ex]].
91. M. J. Leitch, J. Phys. G **34** (2007) S453 [arXiv:nucl-ex/0701021].
92. B. I. Abelev *et al.* [STAR Collaboration], arXiv:1001.2745 [nucl-ex].
93. H. Liu [STAR Collaboration], Nucl. Phys. A **830** (2009) 235c [arXiv:0907.4538 [nucl-ex]].
94. R. Vogt calculations of $R_{\rm dAu}$.
95. E. G. Ferreiro, F. Fleuret, J. P. Lansberg and A. Rakotozafindrabe, arXiv:0912.4498 [hep-ph].
96. A. Adare *et al.* [PHENIX Collaboration], Phys. Rev. Lett. **98**, 232301 (2007) [arXiv:nucl-ex/0611020].
97. R. Vogt calculations of $R_{p\rm Au}$.
98. R. Arnaldi [NA60 Collaboration], talk at ECT* workshop on Quarkonium Production in Heavy-Ion Collisions, Trento (Italy), May 25-29, 2009.